ELM Propagation and Fluctuations Characteristics in H- and L-mode SOL Plasmas on JT-60U

N.Asakura 1), N.Ohno 2), H.Kawashima 1), H.Miyoshi 3), G.Matsunaga 1), N. Oyama 1), S.Takamura 3), Y.Uesugi 4), M.Takechi 1), T.Nakano 1), H.Kubo 1)

1) Japan Atomic Energy Agency, Naka, Ibaraki 311-0193 Japan
2) EcoTopia Science Institute, Nagoya Univ., Nagoya, Aichi 464-8601, Japan
3) Graduate School of Engineering, Nagoya Univ. Nagoya, Aichi 464-8603, Japan
4) Faculty of Engineering, Kanazawa University, 2-40-20 Kodatsuno, Ishikawa 920-8667, Japan

E-mail: asakura.nobuyuki@jaea.go.jp

Abstract. Radial transport of the SOL plasma was recently studied in order to understand heat and particle loading to the first wall. Fast propagation of the ELM plasma and fluctuation properties in H- and L-modes were determined both at high-field-side (HFS) and low-field-side (LFS) SOL using reciprocating Mach probes in JT-60U. Large and short (10-30μs) peaks were found in ELM plasma flux (j_s) mostly at LFS SOL, which was enhanced after each ELM event (magnetic turbulence). Radial propagation of the first large j_s peak was determined with the fast velocity of 1.3-2.5km/s and large decay length of 9 cm. Fast heat and particle transport (and deposition) was measured near the separatrix above HFS baffle (Δr^{mid} < 0.8 cm) just after ELM event, producing the flow reversal due to large particle recycling in the HFS divertor. Statistical analysis of a probability distribution function (p.d.f.) was applied to describe intermittent (non-diffusion) transport in SOL plasma fluctuations. It was found that statistical properties were different between ELMy H-mode and L-mode plasmas. In the ELMy H-mode, positive skewness (i.e. bursty events) was seen in narrow area near the separatrix (Δr^{mid} < 3 cm) both at HFS and LFS SOLs. On the other hand, in the L-mode plasma, bursty events were mostly observed at LFS midplain, which extended to the far SOL (Δr^{mid} < 10 cm), where the "flow reversal" of the SOL plasma was observed. were not extended to the HFS SOL and X-point. Influences of the radial transport of the convective blobby plasma on the SOL formation and the flow reversal were investigated.

1. Introduction

Transient heat and particle loading caused by Edge Localized Mode (ELM) is crucial for determining the lifetime of ITER divertor materials. Radial transport of ELM plasma should be understood to determine the heat and particle fluxes to the first wall. Parallel and radial propagation of the ELM plasma has been investigated in JT-60U [1]. Recently, sampling rate of main edge diagnostics, i.e. three reciprocating Mach probes at Low-Field-Side LFS) midplane, X-point and above High-Field-Side (HFS) baffle, target Langmuir probes, magnetic pick-up coils and D_α emission spectroscopy, was increased to 500 kHz, and the sampling clock was synchronized. Multi peaks in waveform of ion saturation current of the Mach probe (j_s) were identified during ELM events. At the same time, fast TV camera measured time evolution of 2-dimensional image of the divertor plasma with 6-8 kHz.

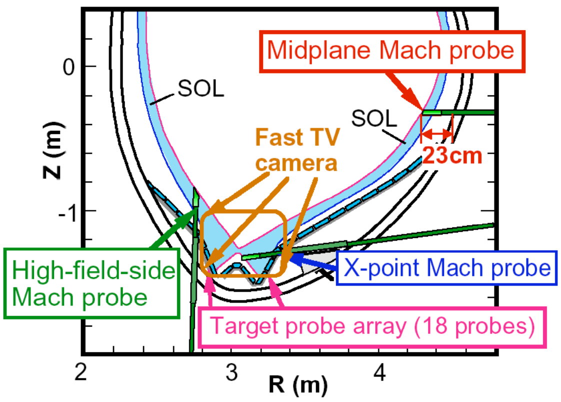

Fig.1 Main diagnostics for SOL and divertor plasma measurements. Three Mach probes measure eadial profiles of SOL plasma at LFS midplane, X-pont and above HFS baffle. Fast TV camera located at midplane port measures devetor tangentially.

Diffusion of the SOL plasma is a fundamental problem. In particular, SOL density at outer flux surfaces (far SOL) was increased in high density

[2]. Recently, non-diffusive transport model was proposed to understand the radial transport [3], and intermittent transport has been observed in edge plasmas [4,5], which may enhance cross-field transport to the first wall. A statistical analysis using a probability distribution function (p.d.f.) can determine non-diffusive events in the fluctuations of tokamak SOL plasmas [6]: when large positive bursts occur frequently more than Gaussian distribution, p.d.f. is positively skewed and more flatten, which are characterized by skewness ($S=\langle x^3\rangle/\langle x^2\rangle^{3/2}$) and flatness ($F=\langle x^4\rangle/\langle x^2\rangle^2$). This method was applied in L- and ELMy H-mode plasmas [7]. Characteristics of the fluctuations in j_s at the important poloidal locations (LFS midplane, X-point and HFS SOL) were determined in L- and ELMy H-modes.

ELM plasma propagation along and across magnetic field lines in the HFS and LFS SOLs is investigated in Sec. 2, and fluctuation characteristics in L- and ELMy H-mode plasmas are compared in Sec.3. Summaries are described in Sec.4.

2. ELM Transport Dynamics in SOL

2.1 Plasma Measurement in Type-I ELMs

ELM plasma propagation was investigated in Type-I ELMy H-mode (I_p =1MA, B_t =1.86T, δ=0.32, κ=1.4, P_{NB} =4.3-5.5MW, $\bar{n}_e$ = 1.8-2.1x10^{19} m^{-3}, large plasma volume of 80m^3). ELM frequency was 20-30Hz, and 10-15 ELMs were measured at the different radius during an insertion of the Mach probe. Figure 2 shows rapid change in magnetic fluctuations ($\tilde{B}_p$) and SOL plasma during an ELM event, i.e. j_s at LFS midplane and divertor strike-point (j_s^{mid} and j_s^{div}), and D_α brightness viewing the main plasma and LFS divertor. Here, distance from the separatrix (Δr^{mid}) for the midplane Mach probe is 4.8 cm, and distance from the strike-point for the target probe corresponds to Δr^{mid} = 0.3cm. Deposition of the heat flux is observed during the enhancement of j_s^{div} by infra-red TV measurement (250μs/frame). Noted that relatively long delay (about 20 μs) in D_α measurement in the previous results [1] was mostly due to separate timing clock for each diagnostic. All clocks for the fast diagnostics are synchronized in this work.

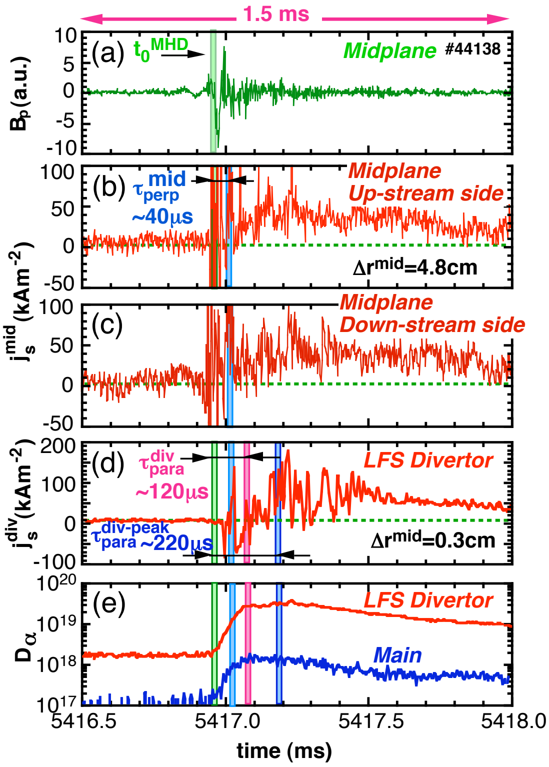

Fig.2 (a) Magnetic fluctuations, midplane j_s (b) at up-stream side and (c) at down-stream side, (d) j_s at LFS divertor, (e) D_α brightness viewing main plasma and LFS divertor.

Amplitude of $\tilde{B}_p$ is largely increased at t =5416.965 ms after a short precursor. The edge turbulence is accompanied with plasma exhaust from edge region [8], and the start of $\tilde{B}_p$ enhancement is defined as t_0^{MHD}. After j_s^{mid} fluctuations, i.e. large positive and negative j_s^{mid} oscillations, multi-peaks of j_s^{mid} appear both at upstream-side (electron drift side) and downstream-side (ion drift side) of the Mach probe: peaks in the upstream j_s^{mid} are seen at t = 5170.005, 5170.044, 5170.110, 5170.152, 5170.218 ms, and those in the downstream j_s^{mid} are slightly different. At the same time, base-level of j_s^{mid} is increased. Here, the first j_s^{mid} peak appears simultaneously at both sides after the large fluctuations (τ_{perp}^{mid} ~40μs), which is defined as delay due to the SOL plasma transport across the magnetic field.

After t_0^{MHD}, a short peak of j_s^{div} is observed at t = 5417.020 ms and amplitude is comparable to the first j_s^{mid} peak, whereas multi-peaks in j_s^{mid} are not observed near the strike point. On the other hand, j_s^{div} base-level starts to increase after t = 5417.080 ms. The delay of the start of j_s^{div} base-level from t_0^{MHD} (= 115 μs) is defined as τ_{para}^{div}. Then, j_s^{div} and D_α brightness become large, and maximum values of j_s^{div} and divertor D_α brightness are observed ~220μs after t_0^{MHD}. Here, plasma convection time from the LFS midplane to the LFS divertor is $\tau_{para}^{SOL\text{-}LFS}$ (= L_s^{LFS}/C_s) =140 μs, where L_s^{LFS} (= 35 m) is the connection length from the LFS midplane to divertor, and C_s is the plasma sound velocity (= 2.5x10^5 m/s) for the pedestal plasma (T_i^{ped}= 800eV and T_e^{ped} = 600eV). Increase in j_s^{div} base-level (τ_{para}^{div}) can be explained by parallel convective transport along the magnetic field lines. It is found that the radial transport of the peak j_s^{mid} is faster than τ_{para}^{div}.

2.2 Radial Propagation of ELM Plasma

Figure 3 shows time evolutions of $\tilde{B}_p$, D_α brightness at the main plasma edge and j_s^{mid} for two ELMs: near separatrix (Δr^{mid} = 1 cm) and at outer flux surface (Δr^{mid} = 8.5 cm), and delay from t_0^{MHD} is shown. Enhancement of D_α brightness starts just after t_0^{MHD}. Multi-peaks in j_s^{mid} often appear after large $\tilde{B}_p$ activities as shown in Fig. 3 (b), i.e. t = 22 and 135 μs, and durations of the two j_s^{mid} peaks are δt^{peak}=15, 22 μs. Base-level of j_s^{mid} is increased after the first j_s^{mid} peak, and it becomes the maximum similar to waveform of the D_α brightness. On the other hand, in the far SOL, j_s^{mid} peak is comparable to that near separatrix, while base-level of j_s^{mid} is small. Characteristic time of the radial propagation is investigated as time lags of the first j_s^{mid} peak and maximum base-level, τ_{perp}^{mid}*(peak)* and τ_{perp}^{mid}*(base)*, respectively.

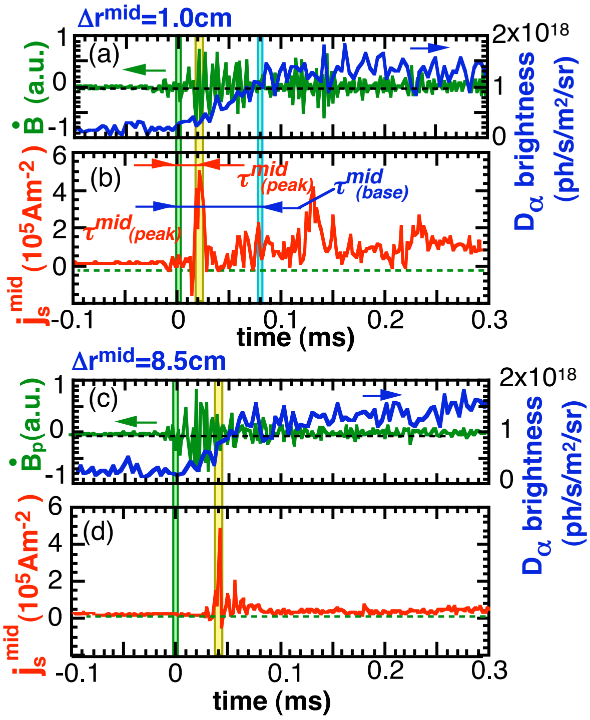

Fig.3 Time evolutions of δB_p, D_α brightness in main plasma, j_s^{mid} at Δr^{mid} =1.0 cm and 8.5 cm, as a function of time lag from t^{MHD}.

Figure 4 shows radial distributions of j_s^{mid} peaks and maximum base-levels, where field lines at Δr^{mid} > 12 cm are connected to upper LFS first wall. The distribution of j_s^{mid}*(peak)* is *an envelope of* j_s^{mid} *peaks* rather than a profile at one moment. Enhancement factor of j_s^{mid}*(peak)* compared to j_s^{mid} *base-level between ELMs* is 10-40 over a wide SOL region. It is found that j_s^{mid}*(peak)* propagates to the outer flux surfaces with small reduction in its amplitude: decay length is 9 cm. On the other hand, increment of j_s^{mid}*(base)* is small (2-6 times) and it is observed

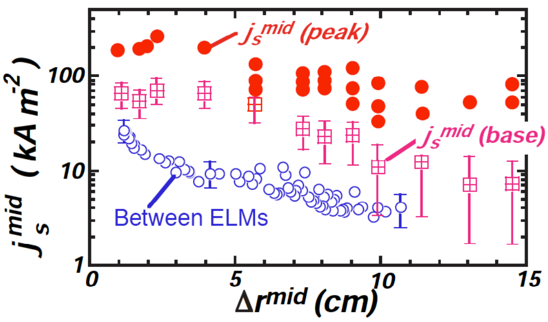

Fig.4 Distributions of j_s^{mid} peaks (closed circle), maximum base-level (square) during ELM, and j_s^{mid} between ELMs (open circle),

at $\Delta r^{mid} < 12$ cm.

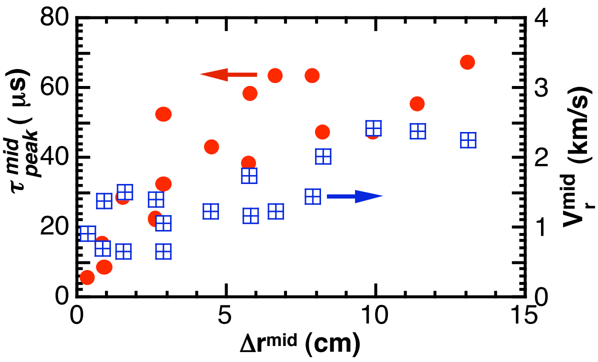

Fig.5 Distributions of $t_{perp}^{mid}(peak)$ and $V_r^{mid}(peak)$ are shown by closed-circles and squares, respectively.

Radial propagation velocity of $j_s^{mid}(peak)$ is evaluated as average velocity from separatrix to the Mach probe location: $V_r^{mid}(peak) = \Delta r^{mid}/\tau_{perp}^{mid}$. Figure 5 shows $\tau_{perp}^{mid}(peak)$ and $V_r^{mid}(peak)$ as a function of Δr^{mid}. Since $\tau_{perp}^{mid}(peak)$ increases with Δr^{mid} near separatrix ($\Delta r^{mid} < 4$ cm), $V_r^{mid}(peak)$ ranges between 0.6 and 1.5 km/s. $V_r^{mid}(peak)$ increases to 1.3 - 2.5 km/s in the far SOL ($\Delta r^{mid} > 4$ cm). Radial scale of j_s^{mid} peak is estimated from $V_r^{mid}(peak)$ and δt^{peak}, assuming a dense plasma cell or plasma filament crosses the Mach probe perpendicular to the field lines. From the measurement, i.e. $V_r^{mid}(peak)$ = 0.6 -1.5 km/s and δt^{peak} =15-22 μs near the separatrix, radial scale of plasma cell corresponds to $\delta t^{peak} V_r^{mid}$ = 1 – 3 cm.

In the far SOL, local expansion velocity is faster than V_r^{mid} since τ_{perp}^{mid} ranges between 38 and 70 μs. ELM propagation was measured in the different plasma configuration with small plasma volume of 60 m^3, where separatrix distance from the midplane Mach probe was 30-45cm. For ten ELM events during the probe movement, τ_{perp}^{mid} ranged in 50 – 80 μs independent of Δr^{mid}, which were comparable to those observed in the far SOL (Fig. 5). Mechanism of the rapid propagation in the far SOL is not understood.

$\tau_{perp}^{mid}(base)$ is increased with Δr^{mid} near separatrix ($\Delta r^{mid} <$ 4cm), and radial propagation is evaluated to be $V_r^{mid}(base)$ ~0.2 km/s. In the far SOL, $\tau_{perp}^{mid}(base)$ is constant (150-200 μs), and plasma propagation is not determined similar to propagation of $j_s^{mid}(peak)$. Here the time lag is comparable to delay of j_s peak at the LFS divertor ($\tau_{para}^{div\text{-}peak}$ = 130-200 μs). Such time scale is comparable to neutral transport with relatively high energy of 10-20 eV, neutral recycling may be a candidate.

2.3 ELM Plasma Transport in HFS SOL

Plasma transport in HFS SOL plays an important role on particle control, impurity transport and tritium retention. Effects of the plasma drifts and the SOL flow on the divertor plasma and impurity transport have been understood in L-mode plasmas on many tokamaks [9,10,11]. On the other hand, ELM plasma dynamics in the HFS SOL and divertor was not understood due to few diagnostics and difficulty of measurement during ELM. ELM dynamics in the HFS SOL and divertor was recently investigated.

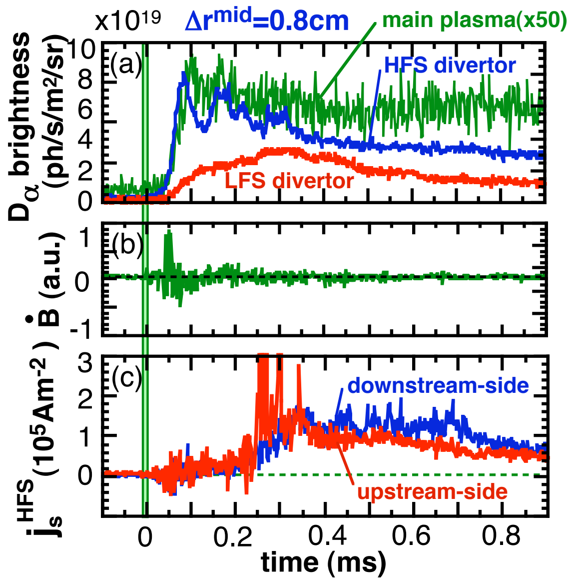

Fig.5 Time evolutions of (a) D_a brightness in main plasma and divertor, (b) δB_p, (c) j_s^{HFS} measured at the up- and down-stream sides of the HFS Mach probe for Δr^{mid} =0.8 cm, as a function of time lag from t^{MHD}.

Figure 5 shows time evolutions of D_α brightness at the main plasma and divertor, $\tilde{B}_p$, and j_s measured at upstream and downstream sides of the HFS Mach probe ($j_s^{HFS\text{-}up}$ and $j_s^{HFS\text{-}down}$) during an ELM. Distance from separatrix to the Mach probe was 3 cm, corresponding to LFS midplane radius of 0.8 cm. D_α brightness viewing the main plasma and divertor start increasing simultaneously after large magnetic turbulence. Start of j_s^{HFS} increase is delayed by ~200μs. During early period (t = 200-300 μs), $j_s^{HFS\text{-}up}$ is larger than $j_s^{HFS\text{-}down}$, which shows the SOL flow towards the HFS divertor with Mach number of the subsonic level (~0.5), calculated from Hutchinson's formula [11]: $M_{//} = 0.4\, ln[j_s^{up}/j_s^{down}]$. Noted that the fast SOL flow is seen only near the separatrix (Δr^{mid} < 1cm). Increase in $j_s^{HFS\text{-}up}$ and the fast SOL flow can be explained by parallel convective transport from LFS SOL since the delay of $j_s^{HFS\text{-}up}$ is comparable to convection time to the HFS Mach probe is $\tau_{para}^{SOL\text{-}HFS}$ (= L_s^{HFS}/C_s) = 240 μs, where L_s^{HFS} (= 60 m).

Enhancement of D_α emission at the HFS divertor starts before the characteristic time of the convective transport. For Δr^{mid} = 0.4 cm (very close to the separatrix), enhancement of j_s^{HFS} starts 45μs after t^{MHD}, and j_s^{HFS} is saturated due to discharge of the Mach probe electrodes as shown in Fig. 6. It is caused by large heat load to the Mach probe. The heat flux may be caused by conduction or fast electrons, and which generates immediate enhancement of particle recycling near the HFS strike-point.

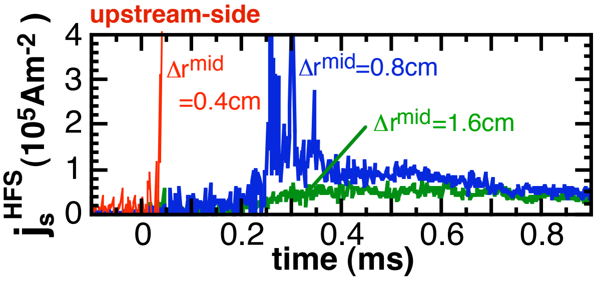

Fig.6 Time evolution of j_s^{HFS} at upstream side of the HFS Mach probe for Δr^{mid} =0.4, 0.8, 1.6 cm, as a function of time lag from t^{MHD}.

During the latter period of j_s^{HFS} enhancement (t = 350-800 μs) in Fig. 5(c), flow reversal (SOL flow away from the HFS divertor) is observed. Figure 7 shows profiles of $j_s^{HFS\text{-}up}$ and Mach number at and after the $j_s^{HFS\text{-}up}$ peak (or maximum). In between ELMs, the flow velocity towards the HFS divertor/baffle is from zero (near separatrix) to 0.7-0.8 (in the outer flux surfaces, where Mach probe is entering the pre-sheath region of the HFS baffle). At $j_s^{HFS\text{-}up}$ peak, plasma density is increased over all inner SOL (from separatrix to HFS baffle) as shown in Fig.7(a). The flow reversal is generally observed in a wide area of outer flux surfaces (1 cm < Δr^{mid} < 3 cm). It is generated by large increase in particle recycling due to rapid heat load near the strike-point and due to convective plasma transport from the LFS SOL.

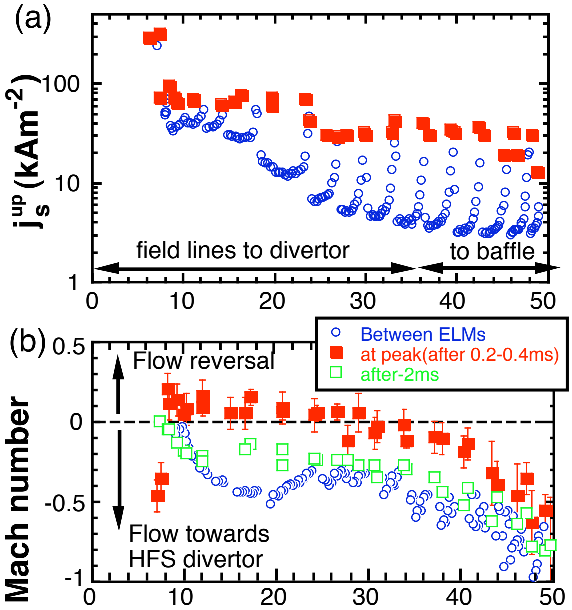

Fig.7 Radial profiles of (a) j_s(upstream-side) above HFS baffle, and (b) Mach number. Profiles are mapped to LFS midplane radius. j_s is saturated Δr^{mid} < 0.7 cm since discharge of the electrode was generated during ELM.

The change in j_s is accompanied with a reduction in the line-averaged electron density at the HFS edge of the main plasma: n_e(0.8a) starts decreasing gradually after the ELM event. Slow increases in both j_s^{HFS} are also affected by the gradual particle loss from the HFS plasma edge.

2.4 ELM Plasma Images in Divertor

Dynamics of ELM plasma (particle recycling and plasma) in the divertor was also investigated, using fast TV camera system. Images of visible light is mostly from D_α emission, and they were measured from a tangential port as shown in Fig. 8. Here, each image is an integral of emission during 330 μs. HFS and LFS strike points are below viewing port edge, and images in HFS and LFS divertors may be identified by in-out asymmetry in light intensity, i.e. larger recycling in the HFS divertor.

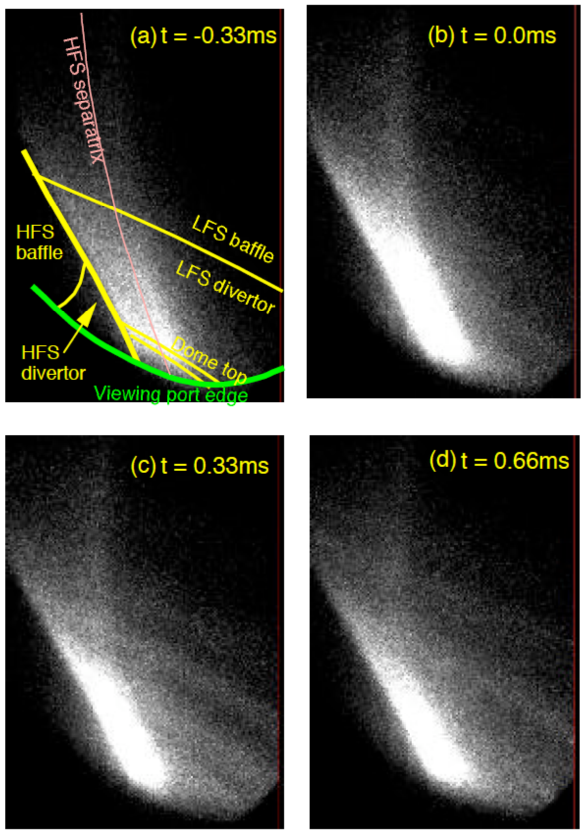

Fig.8 fast TV images of divertor recycling, viewing from midplane tangential port. (a) Divertor geometry is illustrated, with image just before ELM event. Image of particle recycling changes during ELM event: t = (b) 0.0ms, (c) 0.33ms, (d) 0.67 ms.

When ELM event occurs, both emissions from HFS and LFS divertors are increased as shown in Fig.8 (b). Particle recycling above the HFS baffle as well as in the divertor is increased, then the intensity is decreased as shown in Fig.8 (c) and (d). On the other hand, in the LFS divertor, some bright lines are observed along the field lines: 4 and 3 lines are seen in Fig.8 (c) (d), respectively. Number of the lines change during ELM and intensity is increased. Time evolutions of the recycling image (in-out asymmetry) are consistent with the D_α intensities shown in Fig. 6 (a). At the LFS divertor, multi-peak in j_s are observed at the X-point, but the time of the j_s peaks are not correlated to the fast TV image since structure of filaments is not troidally symmetrical.

3. Intermittent transport in SOL fluctuations:

SOL density at outer flux surfaces is increased at high density, forming a flat far SOL. Fluctuation levels (δj_s/<j_s>), statistical properties such as skewness and flatness in j_s^{mid} , j_s^{HFS} and j_s^{Xp} were compared in ELMy H-mode and L-mode plasmas as shown in Figs 9 and 10, respectively. For the L-mode, B_t = 2.7T was higher, $\bar{n}_e$ = 1.7x10^{19} m^{-3} was slightly lower, and P_{NB} = 4MW was lower than those for the ELMy H-mode. Density range was relatively low: $\bar{n}_e/n^{GW}$= 0.42-0.48. Gas puff of 2-5x10^{21} D/s was injected during the L-mode measurement, using density feedback control. Here, δj_s and <j_s> are R.M.S. and average value of j_s during 4 ms. Data between ELMs are used for ELMy H-mode.

SOL plasma density is generally low for the ELMy H-mode plasma. In ELMy H-mode, fluctuation level (δj_s/<j_s>) near separatrix is similar (20-30%) for three probe locations. On the other hand, for the L-mode δj_s/<j_s> becomes large (40-60%) at the LFS midplane and small (10-20%) at the HFS SOL and LFS X-point. As a result, poloidal asymmetry in δj_s/<j_s> is enhanced at the LFS midplane in the L-mode SOL.

It is found that statistical properties are also different between ELMy H-mode and L-mode plasmas. In the ELMy H-mode, positive skewness is seen in narrow area near the separatrix (Δr^{mid} < 3 cm) both at HFS and LFS SOLs. Here, skewness near the X-point is larger than that at the LHS midplane. On the other hand, in the L-mode plasma, large positive skewness is mostly observed at LFS midplane and it is extended to the far SOL (Δr^{mid} < 10 cm). Similar tendency is also seen in flatness profiles. Positive burst signals appeared in the time evolution of j_s^{mid} during short period of less than 25μs without specific frequency spectrum. As a result, turbulences are generated only at LFS SOL (near midplane), which do not propagate to the HFS SOL and X-point (and divertor).

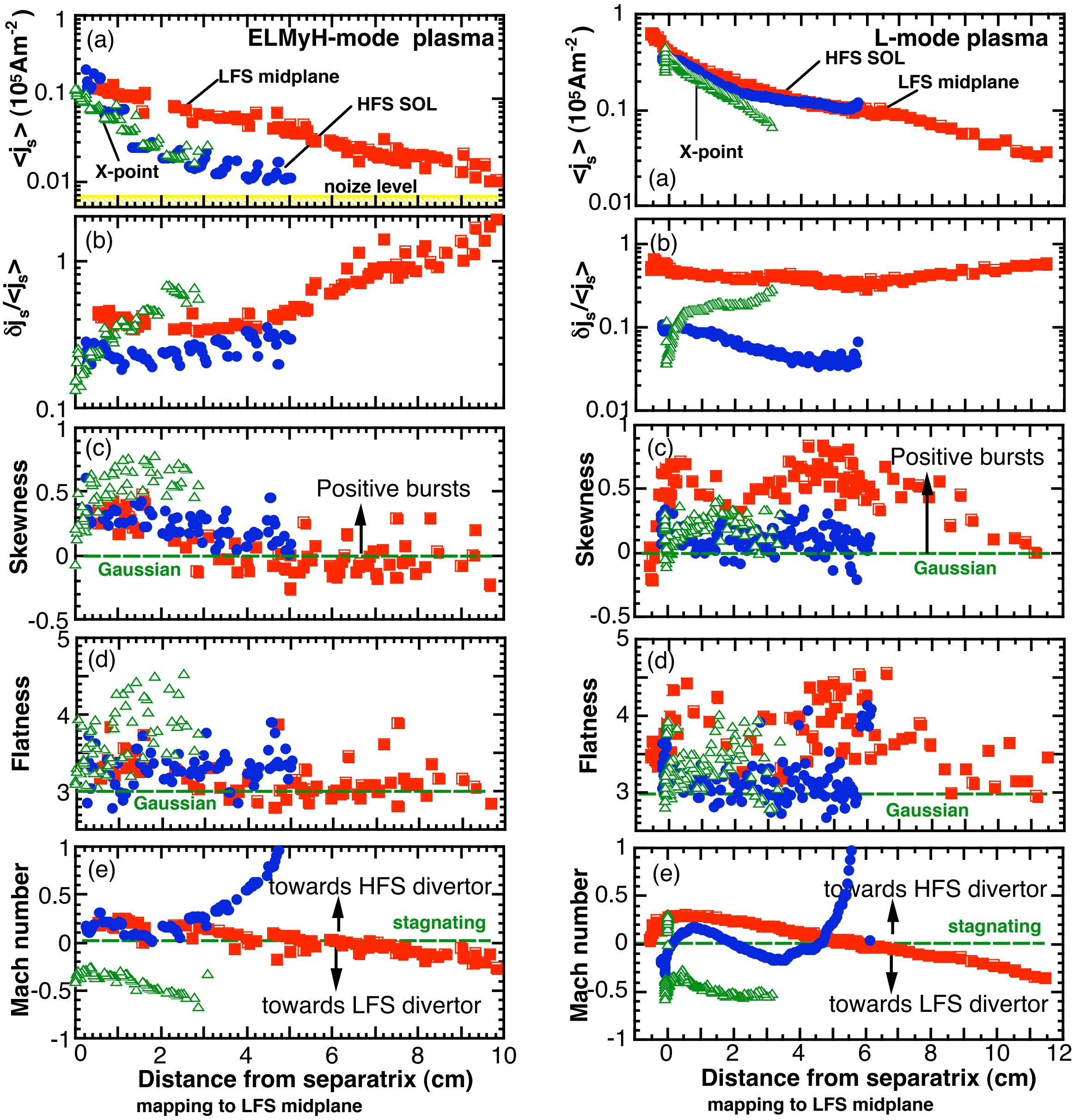

Fig.9 (left) and Fig. 10 (right): profiles SOL plasma and statistical properties in ELMy H-mode and L-mode plasmas, respectively. (a) j_s profiles measured with LFS midplane (squares), HFS (circles) and LFS X-point Mach probes. (b) fluctuation level of j_s, (c) Skewness, (d) Flatness, (e) Mach number of parallel plasma flow. HFS baffle and LFS divertor target are located at the flux surface of 5 cm and 3.2 cm LFS midplane distance, respectively.

"Flow reversal" of the SOL plasma is also observed only at the wide area of the LFS midplane both in L- and ELMy H-modes [13]. It is found that Mach number of the flow reversal in the L-mode (~0.3) is larger and the area (Δr^{mid} < 6 cm) is wider than those in ELMy H-mode ($M_{//}$ ~0.2 and Δr^{mid} < 4 cm). Intermittent radial transport also appears frequently in the wide area of Δr <10cm, and the plasma cell may not propagate to the HFS SOL nor the LFS divertor. This result suggests that the intermittent transport increase the plasma pressure at LFS SOL, which is a candidate mechanism to produce the SOL flow towards the HFS SOL and divertor.

4. Summary

Parallel and perpendicular transport of the SOL plasma was investigated in HFS and LFS SOLs. Fast propagation of the ELM plasma and fluctuation properties in H- and L-modes were determined both at HFS and LFS SOLs using reciprocating Mach probes in JT-60U. Large and short (10-30μs) peaks were found in ELM plasma flux (j_s) mostly at LFS SOL, which was enhanced just after each ELM event (magnetic turbulence). Dynamics of the first large j_s peak was determined: it propagated to near the LFS first wall with $V_{perp}^{mid}(peak)$ = 0.6-1.5 km/s near the separatrix (Δr^{mid} < 4 cm) and $V_{perp}^{mid}(peak)$ is increased to 1.3-2.5 km/s in the far SOL (Δr^{mid} > 4 cm) with large decay length of 9 cm. Filament structure (3-4 lines) reached in the LFS divertor X-point and divertor plate.

Dynamics of the HFS divertor plasma was investigated. Fast and large heat flux was transported in the narrow region near separatrix (Δr^{mid} < 0.8 cm), which mostly produced early enhancement of the particle recycling in the HFS divertor. Then, flow reversal was produced (at least) up to above the HFS baffle.

Statistical analysis of a probability distribution function (p.d.f.) was applied to describe intermittent (non-diffusion) transport in SOL plasma fluctuations. It was found that statistical properties are different between ELMy H-mode and L-mode plasmas. In the ELMy H-mode, positive skewness was seen in narrow area near the separatrix (Δr^{mid} < 3 cm) both at HFS and LFS SOLs. On the other hand, in the L-mode, large positive skewness was observed at LFS midplane and it was extended to the far SOL (Δr^{mid} < 10 cm). However, it does not propagate to the HFS SOL and X-point (and divertor). This result suggests that the intermittent transport increases the plasma pressure at LFS SOL, which may contribute to produce the SOL flow.

Acknowledgments

This research was partly supported by the Grant-in-Aid for Scientific Research (B) 16360463, Japan Society for the Promotion Science.

References

[1] N. Asakura, M. Takechi, N. Oyama, T. Nakano, J. Nucl. Mater. **337-339** (2005) 712.
[2] N. Asakura, Y. Koide, K. Itami, et al. J. Nucl. Mater., **241-243** (1997) 559.
[3] S. Krasheninnikov, Phys. Lett. **A 283** (2001) 364.
[4] J. Terry et al., J. Nucl. Mater. **290-293** (2001) 757.
[5] J.A. Boedo, et al., J. Nucl. Mater. **313-316** (2003) 813.
[6] G.Y. Antar, et al. Phys. Plasmas **10** (2003) 419.
[7] H. Miyoshi, N. Ohno, et. al. 32nd EPS Plasma Physics Conf., Tarragona (2005) P1.045.
[8] N. Oyama, et al., Nucl. Fusion **44** (2004) 582.
[9] W. Fundamenski, P. Andrew, K. Erents, et al., J. Nucl. Mater. **337-339** (2005) 305.
[10] B. LaBombard, J.E.Rice, A.E. Hubbard, et al., Nucl. Fusion, **44** (2004) 1047.
[11] N. Asakura, to submited to J. Nucl.Mater. 2006.
[12] I.H. Hutchinson, Phys. Rev. **A 37** (1988) 4358.
[13] N. Asakura, S. Sakurai, N. Hosogane, et al. Nucl. Fusion 39 (1999) 1983.